JOURNAL OF COMPUTATIONAL PHYSICS 65, 227–243 (1986)

Predictions of Fluid Flow and Heat Transfer Problems by the Vorticity–Velocity Formulation of the Navier–Stokes Equations

TORU FUSEGI AND BAKHTIER FAROUK

Department of Mechanical Engineering and Mechanics, Drexel University, Philadelphia, Pennsylvania 19104

Received May 1, 1985; revised October 16, 1985

A relatively novel formulation of the Navier–Stokes equations is evaluated for obtaining solutions of 2-dimensional incompressible fluid flow and convective heat transfer problems. A vorticity transport equation along with two Poisson equations for the velocity components and the energy equation are solved by a finite difference scheme. A direct solution procedure is used for solving simultaneously the dependent variables along a grid line, using a block tridiagonal matrix algorithm. As test problems, laminar flow motion and heat transfer in a square cavity and in a horizontal concentric annulus induced by various strength of buoyancy and external shear forces are investigated. The formulation is found to be stable for high Reynolds and Grashof numbers and has features that may be desirable for solving a wide variety of flow and heat transfer problems.

INTRODUCTION

The vorticity-stream function ($\omega - \psi$) formulation has long been used in the formulations of the incompressible, viscous flow problems. Since the early 1970s, there has been a noticeable shift of interest from the vorticity-stream function formulations to primitive variable ($u - v - p$) formulations. An account of both formulations, using finite difference methods, is well documented by Roache [1].

The vorticity-stream function formulation has the major advantage of avoiding the continuity equation and the explicit appearance of the pressure. For steady flow, an iteration is usually introduced to handle the vorticity boundary condition at a solid surface. This iteration is in addition to the iteration required to solve the nonlinear vorticity transport equation. The $\omega - \psi$ formulation has serious limitations in calculating flows within multiply connected bodies where the mass flow rate is not known a priori [2]. Also the calculation of vorticity at the solid walls requires the evaluation of a second-order derivative of the stream function at the wall. Finite difference primitive variable formulations have been used with success by several investigators [3–5]. The $u - v - p$ formulations for incompressible flows suffer from the limitation that there are no obvious equations for obtaining the pressure and difficulties in specifying the boundary condition for the pressure at solid walls.

0021-9991/86 $3.00

A relatively novel formulation which alleviates most of the drawbacks mentioned above by employing the vorticity and velocity components is investigated in detail here for solving viscous incompressible fluid flow and heat transfer problems. The formulation has previously been used by Fasel and co-workers [6–8] for solving hydrodynamic stability problems and by Dennis *et al.* [9] for a 3-dimensional fluid flow problem for relatively low Reynolds number ranges. Though the formulation was used with success in the above cases, it has been rarely used in the prediction of convective heat transfer problems. An extensive search revealed that Schonauer *et al.* [10] had applied the formulation to the natural convection problem in a square cavity. Very little heat transfer information is, however, reported in the paper. No detailed flow or temperature field solutions are presented either. It has been observed that the above formulation gives poor results when a sequential "one variable at a time" type iteration procedure is employed. This is particularly the case for high Reynolds or Rayleigh number flows. When point or line-by-line iteration schemes (with a sequential, "one variable at a time" type approach) are employed, the vorticity boundary conditions at solid walls lag behind the iteration cycle as the velocity values at the near wall nodes have to be obtained from the previous iteration. This drawback is eliminated in the direct solution procedure employed here. The vorticity and velocity components (including the boundary values) are solved simultaneously along a given grid line. This type of direct solution procedures are quite common in aerodynamics, but have rarely been used for incompressible viscous flows [11].

The vorticity-velocity formulation ($\omega - u - v$) investigated in this paper has been found to be highly stable for a wide range of Reynold and Rayleigh numbers. Since this is a higher order formulation, it is expected that less restrictive outflow boundary conditions can be considered if such boundaries are present in a given problem. The formulation also appears to be suitable for predicting certain flows within multiply connected bodies, where the net flow rate is not known beforehand.

Test Problems

In order to study the applicability of the formulation, fluid flow and heat transfer problems in a square cavity and horizontal concentric annulus are considered. For the square cavity, the coordinate system is defined in Fig. 1. An insulated top wall (moving or stationary) is considered and the left and right vertical walls are differentially heated to maintain constant temperatures. The bottom wall is also taken to be insulated. For the annulus problem shown in Fig. 2, the inner and outer cylinders are considered to be the isothermal surfaces. Both stationary and rotating inner cylinders are considered.

Governing Equations

The flow and heat transfer phenomena to be investigated here are described by the complete Navier–Stokes and energy equations for two dimensional laminar

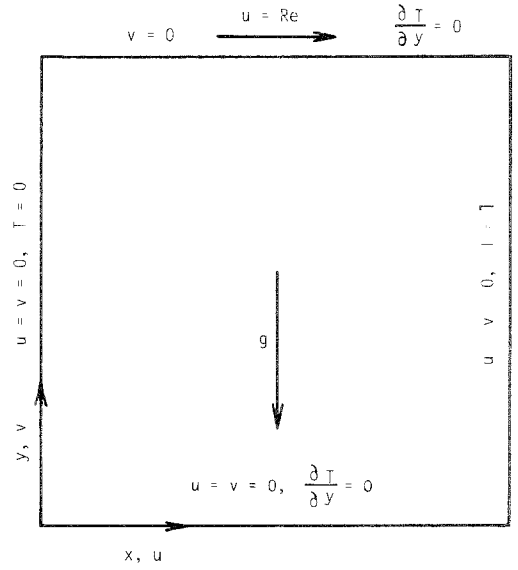

FIG. 1. Geometry and the given boundary conditions for a square cavity.

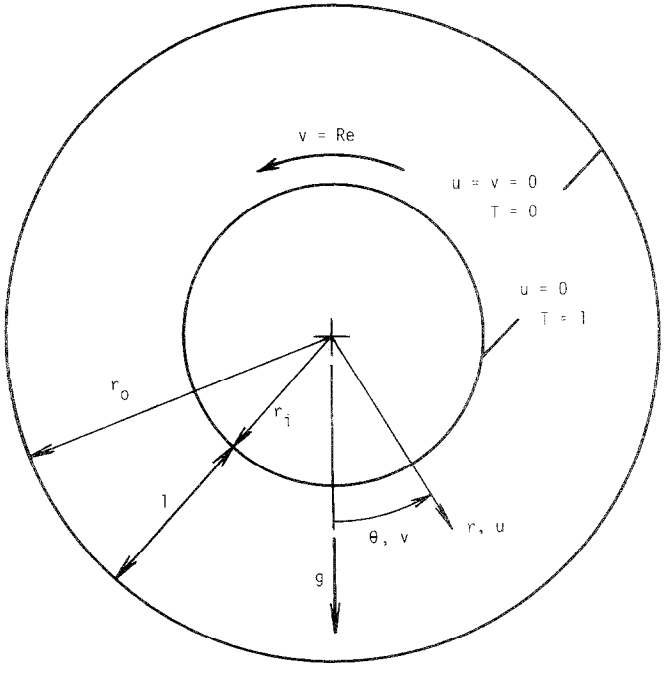

FIG. 2. Geometry and the given boundary conditions for a horizontal concentric annulus.

incompressible flows. The viscous dissipation term in the energy equation is neglected and the Boussinesq approximation is invoked for the buoyancy induced body force term in the Navier–Stokes equations.

In the present formulation, within the framework of the Cartesian coordinate system defined in Fig. 1, the unsteady Navier–Stokes equations are expressed in the vorticity transport form:

$$\frac{\partial \omega}{\partial t}+\frac{\partial}{\partial x}(u\omega)+\frac{\partial}{\partial y}(v\omega)=\frac{\partial^2 \omega}{\partial x^2}+\frac{\partial^2 \omega}{\partial y^2}+\mathrm{Gr}\frac{\partial T}{\partial x} \tag{1}$$

where the vorticity is defined as

$$\omega=\frac{\partial v}{\partial x}-\frac{\partial u}{\partial y} \tag{2}$$

and the continuity equation is given as

$$D=\frac{\partial u}{\partial x}+\frac{\partial v}{\partial y}=0. \tag{3}$$

The two Poisson equations for the velocity components are expressed as

$$\frac{\partial^2 u}{\partial x^2}+\frac{\partial^2 u}{\partial y^2}=-\frac{\partial \omega}{\partial y} \tag{4}$$

and

$$\frac{\partial^2 v}{\partial x^2}+\frac{\partial^2 v}{\partial y^2}=\frac{\partial \omega}{\partial x}. \tag{5}$$

The energy equation is similar to the vorticity equation (1) and can be expressed as

$$\frac{\partial T}{\partial t}+\frac{\partial}{\partial x}(uT)+\frac{\partial}{\partial y}(vT)=\frac{\partial}{\partial x}\left(\frac{1}{\mathrm{Pr}}\frac{\partial T}{\partial x}\right)+\frac{\partial}{\partial y}\left(\frac{1}{\mathrm{Pr}}\frac{\partial T}{\partial y}\right). \tag{6}$$

The two Poisson equations can be derived from the definition of vorticity, Eq. (2), by differentiating it with respect to y and x respectively, and by making use of the continuity condition (3). Equations (1) along with (4)–(6) represent the governing equations in the vorticity–velocity formulation to study the incompressible viscous flow problems. For a given problem the above coupled equations system needs to be solved along with appropriate boundary conditions. The vorticity boundary conditions at the walls introduce additional coupling to the system.

The dependent variables above are given in non-dimensional forms and the variables are defined as follows:

$$x=\frac{x^*}{L}, \qquad y=\frac{y^*}{L}, \qquad u=\frac{u^*L}{\nu}, \qquad v=\frac{v^*L}{\nu},$$

$$\omega=\frac{\omega^*L^2}{\nu}, \qquad T=\frac{T^*-T_C}{T_H-T_C}, \qquad t=\frac{t^*\nu}{L^2},$$

where ν is the kinematic viscosity of the fluid, L is the cavity length, T_H and T_C are the right and left vertical wall temperatures, respectively. The starred $(*)$ variables denote dimensional quantities.

For the concentric annulus problem the governing equations are written in cylindrical polar coordinates and can be found elsewhere [12].

For the square cavity, the following boundary conditions are used:

$$u=0, \quad v=0, \quad \omega=\frac{\partial v}{\partial x}, \quad T=0 \quad \text{at } x=0,\ 0<y<1,$$

$$u=0, \quad v=0, \quad \omega=\frac{\partial v}{\partial x}, \quad T=1 \quad \text{at } x=1,\ 0<y<1,$$

$$u=0, \quad v=0, \quad \omega=-\frac{\partial u}{\partial y}, \quad \frac{\partial T}{\partial y}=0 \quad \text{at } 0<x<1,\ y=0,$$

and

$$u=\mathrm{Re}, \quad v=0, \quad \omega=-\frac{\partial u}{\partial y}, \quad \frac{\partial T}{\partial y}=0 \quad \text{at } 0<x<1,\ y=1,$$

where the Reynolds number is given as $\mathrm{Re}=UL/\nu$, U being the velocity of the moving wall.

For the cylindrical annulus problems, whose dependent variables are non-dimensionalized with respect to the annulus gap width and the temperature difference between the inner and outer cylinder, the following boundary conditions are specified:

$$u=0, \quad v=\mathrm{Re}, \quad \omega=\frac{1}{r}\cdot\frac{\partial}{\partial r}(rv), \quad T=1 \quad \text{at } r=r_i,\ 0\leqslant\theta\leqslant 2\pi,$$

$$u=0, \quad v=0, \quad \omega=\frac{1}{r}\cdot\frac{\partial}{\partial r}(rv), \quad T=0 \quad \text{at } r=r_0,\ 0\leqslant\theta\leqslant 2\pi,$$

where the rotational Reynolds number is given as $\mathrm{Re}=r_i^*\Omega L/\nu$, Ω being the angular velocity of the inner cylinder, r_i and r_0 are the radii of the inner and outer cylinders, respectively. The angle θ is measured counterclockwise from the downward vertical line. The star $(*)$ denotes a dimensional quantity as before.

The Grashof (Gr) and Prandtl (Pr) numbers are defined as follows:

$$\mathrm{Gr} = \frac{g\beta(T_H - T_C)\, L^3}{\nu^2}$$

$$\mathrm{Pr} = \frac{\nu}{\alpha}$$

where g is the gravitational acceleration, β the thermal expansion coefficient of the fluid, $(T_H - T_C)$ the temperature difference of the isothermal walls of the problems, L the cavity length (for the square cavity) or the gap width (for the annulus), and α thermal diffusivity of the fluid. The constant fluid properties are evaluated at the average temperatures of the isothermal walls.

A disadvantage of the $(\omega - u - v)$ system, when compared to the $(\omega - \psi)$ system, is that storage for one more variable and, therefore, one additional 2-dimensional array is required for the steady as well as the unsteady problem. However, with respect to storage this system is equivalent or even superior to the $(u - v - p)$ system, since the steady problem requires the same number of arrays while the unsteady problem calls for fewer arrays. An advantage of the present formulation over the $(\omega - \psi)$ system is that the velocity components u and v are readily available when required, e.g., for the transient period in unsteady flow problems.

There are certain aspects of this formulation that require special attention [6]. Although continuity was assumed to be satisfied for derivation of Eqs. (4) and (5), it is not necessarily guaranteed for the difference equations based on the $\omega - u - v$ formulation. Differentiating Eqs. (4) and (5) for x and y, respectively, and adding the resulting equations, it can be shown that

$$\frac{\partial^2}{\partial x^2}(D) + \frac{\partial^2}{\partial y^2}(D) = 0. \tag{7}$$

From the "maximum principle" it follows that $|D|$ is maximal on the boundary. Thus it can be concluded that continuity $(D = 0)$ is guaranteed in the entire integration domain if it is satisfied on the boundary. Thus, if care is taken to satisfy the continuity condition to a high degree of accuracy on the boundaries, mass conservation is guaranteed to even higher accuracy in the interior of the integration domain. Similar consideration applies to the vorticity definition. It should be noted that for the class of problems investigated in the present paper, the continuity condition is automatically satisfied on the boundaries by the presence of no-slip walls.

Solution Method

A direct solution method (along a grid line) is presented here for solving the system of coupled differential equations via a block tridiagonal matrix algorithm. The set of governing equations is discretized by a control-volume based finite dif-

ference method. The convective terms are approximated by a hybrid differencing scheme [13] and a fully implicit transient scheme is employed. It is seen that the vorticity and velocity equations (1) and (4)–(5) are coupled and there is an additional coupling through the wall boundary conditions. However, the energy equation (6) is coupled to the vorticity and velocity equations by the source term in the vorticity equation and the convection terms in the energy equation itself. The finite difference approximate equations to these flow problems must be solved iteratively. This is usually accomplished by the linearization process of employing the results of previous iteration in calculating the coefficients of the non-linear convective terms. In the present application of interest in the vorticity–velocity formulation, the difference equations are solved directly for a given line of grid points at constant x (or constant θ for the polar coordinate). The discretized system can be thought of as an ensemble of several tridiagonal subsystems coupled through diagonal submatrices. The system has the form:

$$a^l_{i,j}\phi^l_{i,j-1} + b^l_{i,j}\phi^l_{i,j} + c^l_{i,j}\phi^l_{i,j+1} + \sum_{\substack{k=1 \\ k\neq l}}^{m} (a^k_{i,j}\phi^k_{i,j-1} + b^k_{i,j}\phi^k_{i,j} + c^k_{i,j}\phi^k_{i,j+1}) = e^l_{i,j} + f^l_{i,j}(\phi^l_0)_{i,j} \tag{8}$$

where the indices i and j represent spatial location and ϕ^l_0 denotes the values of the associated dependent variable ϕ^l at the previous time level. The above equation is written for each dependent variable ϕ^k ($k = 1, 2,..., m$, where m is the number of the dependent variables). The vorticity boundary conditions along the walls at constant x (or θ) can also be cast into the above form, with forward or backward finite difference expressions of the second-order accuracy. The resulting equation set forms a block-tridiagonal system for the given grid line of constant x (or θ), to which a block-tridiagonal matrix algorithm is applied to obtain a solution. It is to be noted that along the given grid line all values of ϕ^k are considered at the same iteration level. The solution of the whole domain is obtained by applying the above solution algorithm consecutively to all the grid lines in the positive x (or θ) direction, and then, the sweep direction is reversed. To accelerate convergence, the discretized equation set with a similar form to Eq. (8) can also be formed along grid lines of constant y (or r) and the above two-way sweeping is performed. This four directional sweep is especially important for the square cavity problem where walls are present along both constant x and y lines.

The iteration is terminated when values of the dependent variables at each grid point satisfy the following convergence criterion:

$$\text{maximum}\,|(\phi^k_n - \phi^k_{n-1})/(\phi^k_n)_{\text{maximum}}| \leqslant 10^{-5} \qquad (k = 1, 2,..., m),$$

where ϕ^k stands for any dependent variable, and n the iteration level. Also, an energy balance check was performed before the iteration scheme is terminated. The mean Nusselt numbers of the cold and hot walls agreed to 1% or better for all the

cases studied here. In addition, calculations were made to ensure the satisfaction of the mass balance conditions in the entire domain for all the computations in order to validate the self-consistency of the present formulation. In all cases mass balances were satisfied within 0.05%.

Results and Discussions

Results were obtained for forced, free, and mixed convection problems in a square cavity and free and mixed convection problems in the cylindrical annulus using the $(\omega - u - v)$ formulation. Although the computations were carried out with a fully implicit scheme in time, only steady state solutions are presented here. In all cases steady states are reached. These results demonstrate the applicability of the vorticity–velocity formulation, which up to now has been ignored by a majority of the investigators in convective heat transfer. The mixed convection problems considered in the cylindrical annulus are significant, as the problem is difficult to analyze in the vorticity-stream function formulation due to the unknown mass flow rate through the cylindrical annulus.

Square Cavity Problem

Forced convection problems were solved first for the square cavity by setting $\mathrm{Gr} = 0$ in the formulation, which decouples the energy equation from the vorticity transport and velocity equations. The driving force of the fluid motion is the sliding top in this case. Although the vorticity at the two upper corners takes an infinite value, the present five-point finite difference method does not suffer from this difficulty. This so-called "driven cavity" problem has been widely used by investigators to evaluate numerical schemes in the past [14, 15]. Curiously, though the hydrodynamic problem has been solved by many researchers, no heat transfer results for the forced convection case could be found in the literature. Nusselt numbers for a similar problem have been reported by Chen *et al.* [16] but different temperature boundary conditions were used in that case. Thus for the forced convection problems, only flow characteristics obtained with the present formulation could be compared with previous studies.

For the forced convection in the square cavity, results were obtained for the Reynolds number ranging from 10^0 to 5×10^3. Constant fluid properties with the Prandtl number value of 0.72 were used for all cases. A 51×51 uniform mesh was employed for the Reynolds number up to 400 and the number of grid points were increased up to 81×81 for Re beyond that value in order to obtain grid independent results with the uniform mesh system. The results obtained for lower Reynolds number cases were used as the initial data of the computation for higher Reynolds number cases. No under-relaxation factor was used for the forced convection studies.

Figure 3 shows the u velocity distributions at the cavity vertical mid-plane $(x = 0.5)$ and v profiles at the horizontal mid-plane $(y = 0.5)$ for $\mathrm{Re} = 400$, 10^3, and

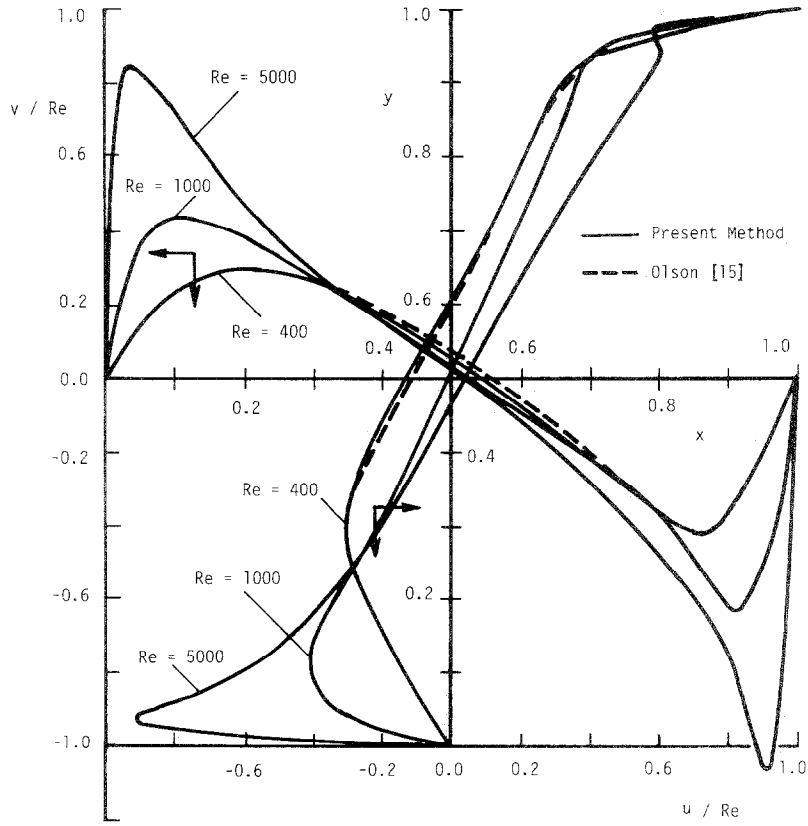

FIG. 3. Profiles of u and v along the cavity vertical and horizontal mid-planes ($x = 0.5$ and $y = 0.5$, respectively) for different moving lid velocities (Re) (Ra = 0).

5×10^3. For lower Reynolds numbers (not shown here) the predictions had excellent agreement with previous studies [17]. The u and v profiles at Re = 400 are compared with the solutions given by Olson [15]. Very good agreements are obtained in this case. No numerical instabilities were observed in the solution procedure.

Figure 4 gives the streamlines (ψ/Re) computed from the velocity field at Re = 1000. The results are in good qualitative agreement with the predictions given by de Vahl Davis and Mallinson [18]. The temperature results in this case could not be compared with previous studies due to the lack of results for the same geometry and temperature boundary conditions in the literature. It was, however, observed that a very large temperature gradient occurs near the hot wall as Reynolds number increases. The local Nusselt number at the hot vertical wall remains fairly uniform for most of the length and then increases rapidly as the moving lid is approached. The cold wall characteristics are different and the Nusselt number peaks only at the middle in this case.

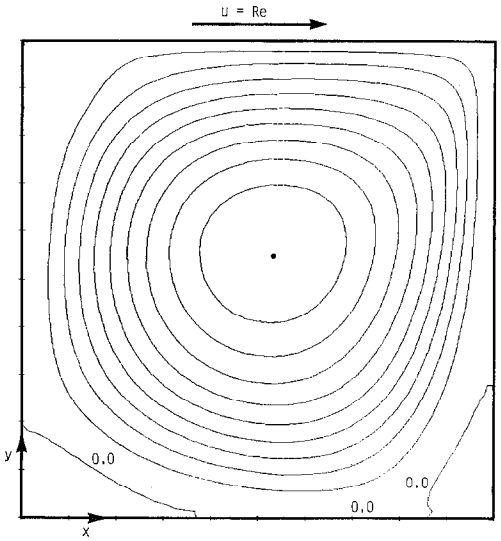

FIG. 4. Stream function (ψ/Re) contours at Re = 1000 ($\Delta(\psi/\mathrm{Re}) = 0.014$) (Ra = 0).

Free convection results in the cavity are presented next, obtained by the vorticity–velocity formulation. The top wall was considered to be stationary and the fluid motion is caused solely by the buoyancy effects. The Rayleigh number Ra ($= \mathrm{Gr} \cdot \mathrm{Pr}$) was varied from 10^2 to 10^6 and a constant Prandtl number of 0.72 was used. A 31×31 mesh was used for the lower Rayleigh numbers and it was gradually increased to 81×81 for the highest Rayleigh number studied. The natural convection results were compared with a recent bench mark numerical solution of the same problem by de Vahl Davis [19]. In general, the agreements of the present solution obtained by the vorticity–velocity formulation with those given in [19] are excellent.

The u and v profiles at the vertical and horizontal mid-sections are shown in Fig. 5 for $\mathrm{Ra} = 10^4$. The profiles are symmetric and the location and magnitude of the maximum values of u and v as given in [19] are also shown in same figure. The agreement appears to be very good. With higher Rayleigh numbers, the velocity peaks move closer to the walls, indicating formation of boundary layers. The isotherms obtained at $\mathrm{Ra} = 10^4$ are plotted in Fig. 6 and they are found to undergo an inversion at the central region of the cavity.

The local Nusselt number (Nu) distributions at the cold and hot walls for various Rayleigh number is shown in Fig. 7. The location and magnitude of maximum Nusselt numbers given in [19] are also shown in the figure. The solution by Jones [20] is also compared with the present solutions and the agreement is found to be good.

The mean Nusselt number ($\overline{\mathrm{Nu}}$) predictions are compared with those given in [19] in Fig. 8. The two sets of predictions almost overlapped each other. No

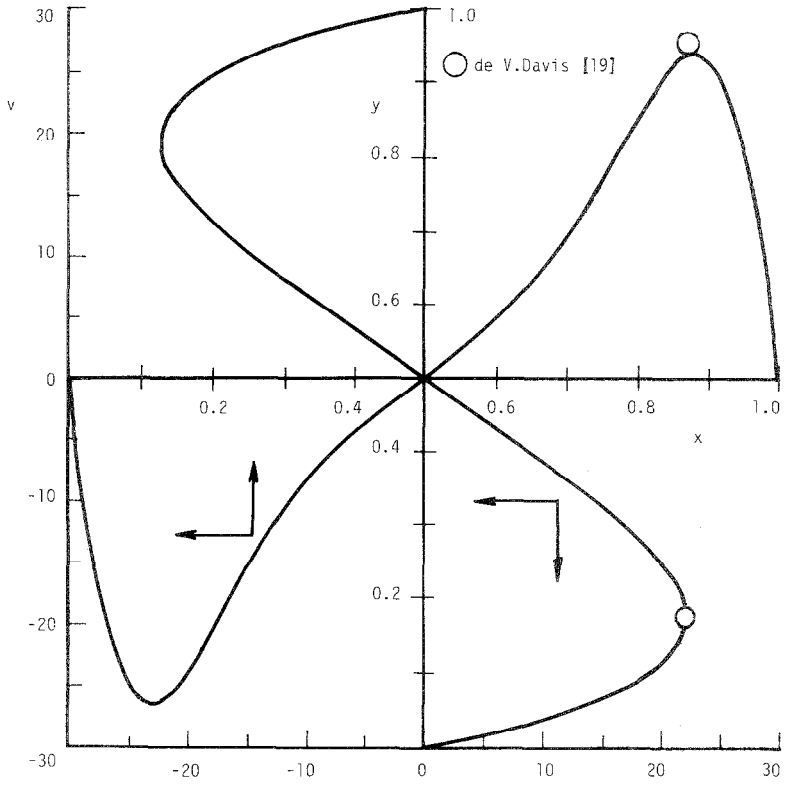

FIG. 5. Profiles of u and v along the cavity vertical and horizontal mid-planes ($x = 0.5$ and $y = 0.5$, respectively) with $\mathrm{Ra} = 10^4$ (natural convection).

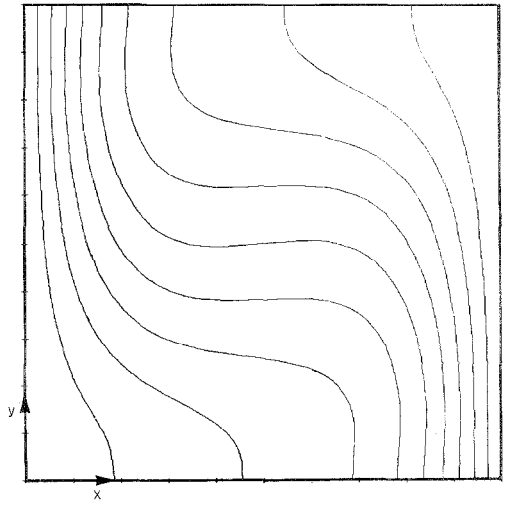

FIG. 6. Isotherms (T) at $\mathrm{Ra} = 10^4$ ($\Delta T = 0.1$) (natural convection).

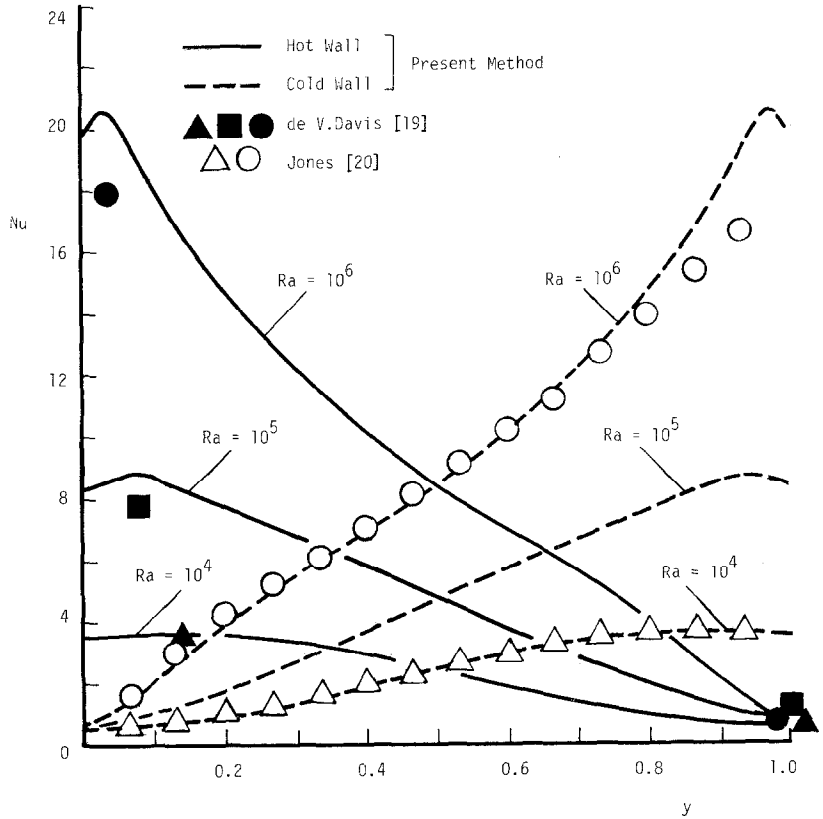

FIG. 7. Distribution of the local Nusselt number (Nu) along the cavity cold and hot walls ($x = 0$ and $x = 1$, respectively) for various Ra (natural convection).

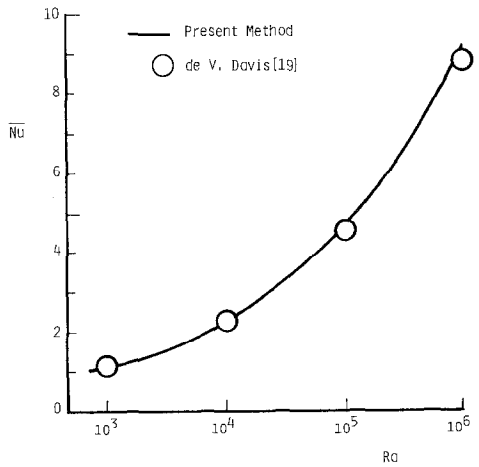

FIG. 8. Change in the average Nusselt number ($\overline{Nu}$) with Ra (natural convection).

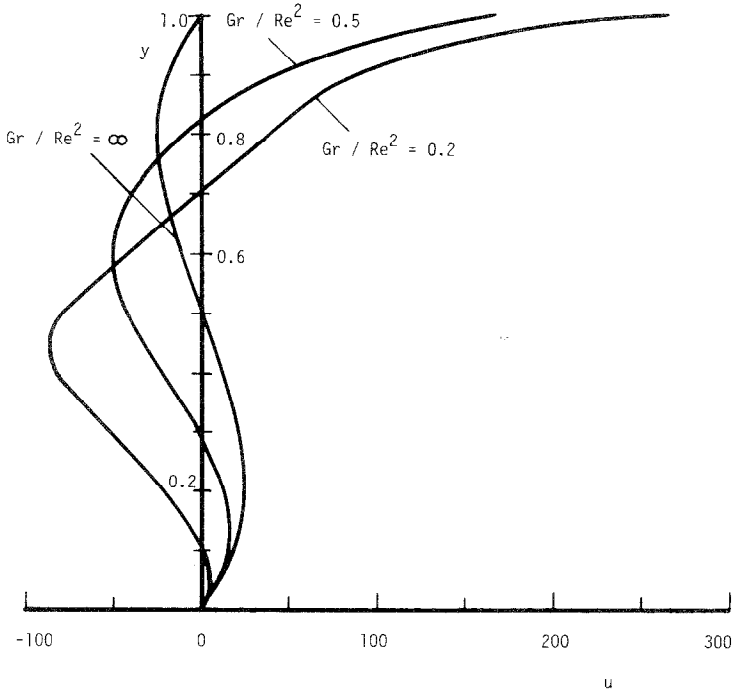

FIG. 9. Profiles of u at the cavity mid-plane ($x = 0.5$) at $\mathrm{Ra} = 10^4$ for various values of $\mathrm{Gr}/\mathrm{Re}^2$.

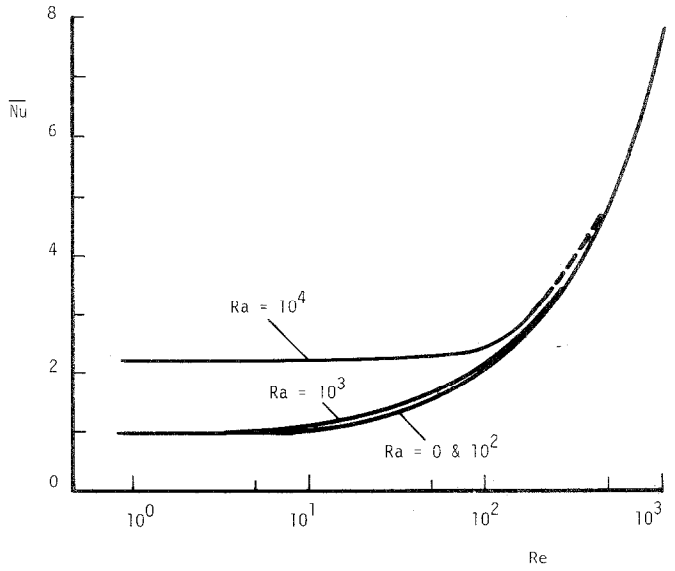

FIG. 10. Distribution of the average Nusselt number as a function of Reynolds number for various values of $\mathrm{Gr}/\mathrm{Re}^2$.

solutions above $Ra = 10^6$ were attempted as the flow may no longer be laminar and stable in those cases.

The mixed convection results obtained with the vorticity–velocity formulation are presented in Figs. 9 and 10. Unfortunately, no past work could be found in the literature for mixed convection problems with the geometry and boundary conditions studied here. The u velocity distributions at the vertical mid-plane are shown in Fig. 9 for the mixed convection problem at $Ra = 10^4$. Due to the buoyancy induced flow, two cell appear for $Gr/Re^2 = 0.2$ (Compare with Figs. 3 and 5). The mean heat transfer characteristics of the mixed convection problems studied are shown in Fig. 10. The mean Nusselt number is plotted against the Reynolds number for various Rayleigh numbers. The forced convection results are also shown for comparison. For the range of parameters studied, the Nusselt number predictions at $Ra = 10^2$ were not much different from those at $Ra = 0$ (forced convection). At higher Reynolds numbers, the predictions for different Ra approached the forced convection values, as expected. No comparisons with published data, however, could be made due to the lack of such results in the literature.

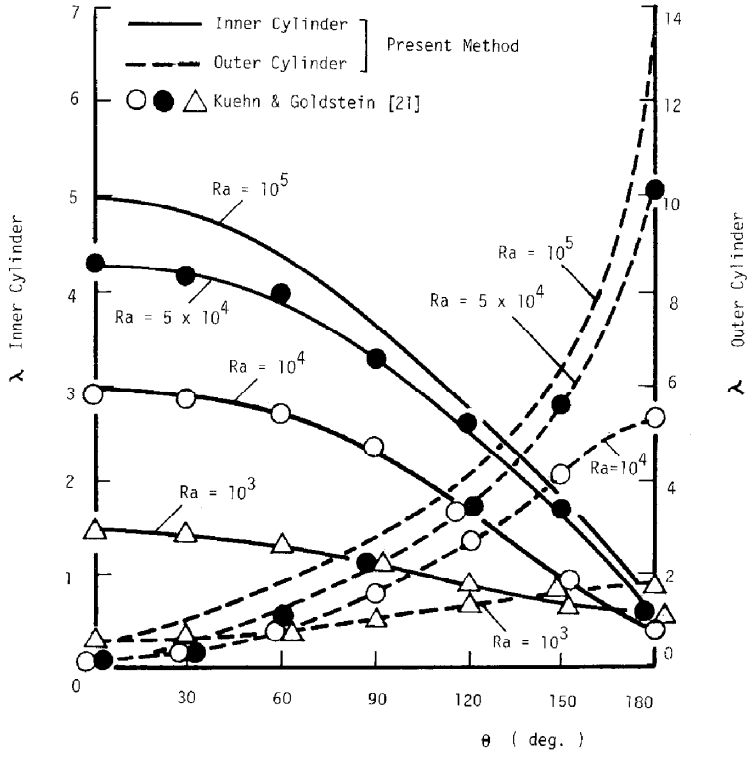

FIG. 11. Distributions of the local equivalent conductivity (λ) on the inner and outer cylinder surfaces for various values of Ra.

Annulus Problem

Natural convection in the annulus between the concentric cylinders is investigated next. The ratio of the gap width to the inner cylinder diameter is held fixed at 0.8. The stationary inner cylinder is considered first. The direction of the gravitational force is taken as $\theta = 0°$. The Rayleigh number, defined with the gap width and the temperature difference of the two isothermal cylinder surfaces, was varied from 10^2 to 10^5. Beyond the maximum Ra studied, the flow is thought to become turbulent [21]. The Prandtl number was set at a constant value, 0.72. The entire domain of the annulus was solved without considering symmetry planes. The uniform mesh system was considered and the number of grid points used for the computations was $41(r) \times 72(\theta)$ for Ra up to 10^4 and $51(r) \times 84(\theta)$ for Ra beyond that value. To compute higher Ra cases, solutions for lower Ra are used as the initial guesses of the iterative solution procedure as before. No under-relaxation was necessary for all the cases studied.

The distribution of the local equivalent conductivity (λ) on the cylinder surfaces is shown in Fig. 11. The equivalent conductivity is defined as the actual heat flux devided by the heat flux that would occur by pure conduction in the absence of

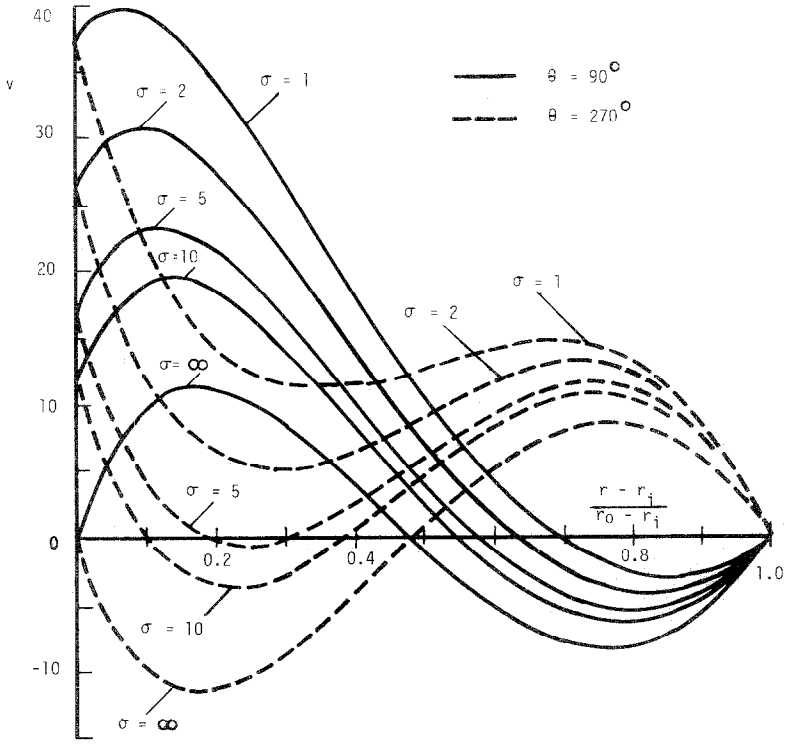

FIG. 12. Angular velocity distributions for the annulus with rotating inner cylinder at $\mathrm{Ra} = 10^3$.

fluid motion. For the inner cylinder, the location of the maximum equivalent conductivity is at the bottom stagnation point and the minimum value occurs at the top stagnation point. At $Ra = 10^3$, the curves for both the inner and outer cylinders lay about $\lambda = 1$, which indicates that heat transfer is in the conduction regime. However, for Ra over 5×10^4, sharp peaks of λ appear at the top region of the outer cylinder due to the presence of impinping plumes there. The results in [21] are also plotted in the figure and show good agreement with the present predictions.

Finally, results for mixed convective flows in the annulus are presented where the heated inner cylinder is rotating. The net flow rate through the annulus is not known a priori for various combinations of the Grashof and rotational Reynolds number. The vorticity-stream function formulation is unsuitable for problems of this class [12]. The vorticity–velocity formulation along with the block tridiagonal matrix algorithm was found to give good results in this case. It can be shown that the parameter $\sigma = Gr/Re^2$ determines the relative strength of the effects of the buoyancy and centrifugal forces in the above problem. The pure natural convective flows reported earlier correspond to the case $\sigma = \infty$. Figure 12 displays the radial angular velocity profiles at $Gr = 1.39 \times 10^3$ ($Ra = 10^3$) for various values of σ. The inner cylinder is considered to be rotating counterclockwise and the results are shown for $\theta = 90°$ (the ascending side) and $\theta = 270°$ (the descending side). For the ascending side buoyancy enhances the rotation induced flow whereas it suppresses the flow in the descending side. The average equivalent conductivities were found to decrease slightly for decreasing values of σ. This is because the rate of growth of the thermal boundary layer on the ascending side of the inner cylinder is less rapid than that on the descending side. It is conjectured that the interaction seen between the buoyant and the centrifugal effects could delay the transition to the Taylor-vortex flow [22]. This however, needs further careful study.

Conclusion

The study has successfully demonstrated the applicability of the vorticity–velocity formulation in solving a variety of fluid flow and heat transfer problems in different geometries. A direct solution procedure is used for solving simultaneously (instead of the traditional "one variable at a time" approach) along a grid line using a block tridiagonal matrix algorithm. The formulation also allows relatively easy extension to full three dimensions where six dependent variables (for the Navier–Stokes equations) are required. With the advent of powerful computers, the problem of storage requirement has lessened and the formulation may be attractive due to its other advantages. The formulation is found to give "robust" computer codes which employ standard numerical methods of solution, without requiring any special treatments like "staggered grids."

The computation were carried out on a PRIME 850 computer. The approximate number of iterations required for convergence at each time level varies from 100 to 500 depending on the values of the Reynolds and Rayleigh numbers of the

problems as well as on the number of grid points. Typical CPU times varied from thirty minutes to three hours.

ACKNOWLEDGMENT

This material is based upon work supported by the National Science Foundation under Grant MEA-83075606.

REFERENCES

1. P. J. ROACHE, *Computational Fluid Dynamics* (Hermosa, Albuquerque, N.M., 1972), Chap. III.
2. B. FAROUK AND S. I. GUCERI, *Numer. Heat Transfer* **5**, 329 (1982).
3. S. V. PATANKAR AND D. B. SPALDING, *Int. J. Heat Mass Transfer* **15**, 1787 (1972).
4. W. R. BRILEY AND H. MCDONALD, AIAA Paper 79-1453 (1979).
5. K. N. GHIA AND J. S. SLKEY, *J. Fluids Eng.* **99**, 640 (1977).
6. H. F. FASEL, *J. Fluid Mech.* **78**, 355 (1976).
7. H. F. FASEL AND O. BOOZ, *J. Fluid Mech.* **138**, 21 (1984).
8. H. F. FASEL, H. BESTEK, AND R. SCHEFENACKER, AGARD-CP-224, Paper 14 (1977).
9. S. C. R. DENNIS, D. B. INGHAM, AND R. N. COOK, *J. Comput. Phys.* **33**, 325 (1979).
10. W. SCHONAUER, K. RAITH, AND G. GLOTZ, in *Numerical Method in Laminar and Turbulent Flow, Venice, Italy, 1981*, edited by C. Taylor and B. A. Schrefler (Pineridge, Swansea, U. K., 1981), p. 943.
11. D. A. ANDERSON, J. C. TANNEHIL, AND R. H. PLETCHER, *Computational Fluid Mechanics and Heat Transfer* (McGraw–Hill, New York, 1983), p. 129.
12. K. S. BALL AND B. FAROUK, in *Advances in Computer for Partial Differential Equations V, Bethlehem, Pa., 1984*, edited by V. R. Vichnevesky and R. S. Stepelman, p. 80.
13. D. B. SPALDING, *Int. J. Numer. Methods Eng.* **4**, 551 (1972).
14. S. G. RUBIN (Ed.), NASA SP-378 (1975).
15. M. D. OLSON, University of British Columbia Civil Engineering Structural Research Series Report 22, 1979 (unpublished).
16. C. J. CHEN, H. NASERI-NESHAT, AND K. S. HO, *Numer. Heat Transfer* **4**, 179 (1981).
17. O. R. BURGGRAF, *J. Fluid Mech.* **24**, 113 (1966).
18. G. DE VAHL DAVIS AND G. D. MALLINSON, *Comput. Fluids* **4**, 29 (1976).
19. G. DE VAHL DAVIS, *Int. J. Numer. Methods Fluids* **3**, 249 (1983).
20. I. P. JONES, in *Numerical Methods in Thermal Problems, Swansea, U.K., 1979*, edited by R. W. Lewis and K. Morgan (Pineridge, Swansea, U.K., 1979), p. 338.
21. T. H. KUEHN AND R. J. GOLDSTEIN, *J. Fluid Mech.* **74**, 695 (1976).
22. G. I. TAYLOR, *Philos. Trans. R. Soc. London A* **223**, 289 (1923).